Supplementary Information for

Collisional excitation of HNC by He found to be stronger than for structural isomer HCN in experiments at the low temperatures of interstellar space

Brian M. Hays,[1] Divita Gupta,[1] Theo Guillaume,[1] Omar Abdelkader Khedaoui,[1] Ilsa R. Cooke,[1] Franck Thibault,[1] François Lique[1] and Ian R. Sims[1,*]

[1] Univ Rennes, CNRS, IPR (Institut de Physique de Rennes) - UMR 6251, F-35000 Rennes, France.

*e-mail: ian.sims@univ-rennes1.fr

List of Supplementary Information:

1 Experimental methods and results

A – Data analysis and fitting

The experimental signal obtained after signal averaging and background subtraction (see Methods section in the main article), consisted of a series of FIDs (free induction decays) recorded as a function of time delay from the firing of the photolysis laser. For HNC, its hyperfine splitting was not resolved under the pressure-broadened experimental conditions, and these signals were fitted with the same time domain Voigt single frequency function as used in Hays et al.,[1] while for HCN this was modified to account for hyperfine splitting. The need for the modified model is exemplified in Fig. 2 of the main article, panels a and c, where the HCN decay profile is visibly more complex due to the beat pattern of the hyperfine components. The new decay function used in this case is given in Supplementary Eq. 1:

$$f(t) = \exp\left(-\frac{t}{T_2} - \frac{\pi^2 \Delta\nu_{Dopp}^2 t^2}{\ln(2)}\right) \times \sum_{n=1}^{N} A_n \cos(2\pi\nu_n t + \theta_n) \qquad \text{Eq. 1}$$

T_2 is the rate of decay due to collisional dephasing, which is related to the pressure broadened linewidth of a spectral transition through $T_2 = 1/2\pi\Delta\nu_{Pres}$, and $\Delta\nu_{Dopp}$ is the Doppler broadening linewidth. A_n, ν_n, and θ_n are the amplitude, frequency, and phase for each hyperfine component, denominated by the *n* subscript. The local frequency fitting parameters were kept fixed to their literature spacings.[2,3] For the *j*=1-0 transition of HCN or any other linear molecules with small hyperfine coupling, the pressure broadening and shifting parameters were found to be the same for each hyperfine component,[4] greatly simplifying analysis. For both molecules, the Doppler component was constrained to the flow temperature, but this only has a minor contribution to the overall decay. This transition is much weaker at 70 K due to Boltzmann scaling. For the data taken at this temperature for HCN, the phase relationship between each hyperfine component was fixed to the values found from fitting the highest signal to noise FID within that dataset.

The cross sections for the experimental data were found using Supplementary Eq. 2:

$$\mathrm{Re}[\sigma(T)] = \frac{2\pi\Delta\nu_{Pres}}{N\langle v\rangle} = \frac{1}{N\langle v\rangle T_2} \qquad \text{Eq. 2}$$

Where T_2 is the fitted decay time, $\sigma(T)$ is the pressure broadening cross section, *N* is the total density in the flow, and $\langle v\rangle$ is the mean relative velocity of the colliding partners. The total density and the temperature are obtained from impact pressure measurements, and the temperature is used to determine $\langle v\rangle$ in the probing region.

Only molecules isolated within the cold uniform flow were included in the pressure broadening data, which could be easily distinguished from molecules produced in the nozzle by time dependent changes of the decay rate at the end of the collected flow data as shown in Fig. 1c. To produce each cross section, the individual T_2 decay times resulting from fitting the FIDs were averaged together, taking the 95% percent confidence interval from the averaged points. Each individual FID resulted from averaging the recorded data from 10^5 laser shots, except for the data at 70 K where 4×10^5 shots were averaged owing to the poorer signal as explained above. Multiple FIDs were also sequentially averaged to increase the signal to noise available per fit, but this blurs the time referencing of the averaged FID in relation to

the laser shot. To reduce any negative effects of this blurring, only 2 to 4 successive FIDs were combined through sequential averaging. The use of very low densities of vinyl cyanide precursor (~0.1% of the total density) ensured that pressure broadening from collision partners other than He could be ignored, as in previous work on rotational energy transfer in uniform supersonic flows.[5,6] The possible effects of heating the uniform supersonic flow due to energy release from the vinyl cyanide dissociation were investigated. However, these are very difficult to quantify owing to uncertainties in the quantum yields of the various channels after photon absorption. Furthermore, when such heating effects have been investigated using the VENOM (vibrationally excited NO monitoring) technique, simple calculations were found to significantly overestimate the actual observed temperature difference.[7] The effect was therefore investigated experimentally at the two lowest temperatures (where it would have the biggest impact) by doubling the vinyl cyanide concentration. No difference was observed in the measured T_2 values outside of the quoted uncertainties, and so it is unlikely that significant heating is occurring.

The overall uncertainties in the temperature and total density in the flow were estimated to be at most 10%, and these were combined with the statistical errors in the values of T_2 to yield the error bars shown in Fig. 3 of the main article, and the values are shown in Supplementary Table 1 below.

B - Experimental conditions and results

T (K)	N (10^{16} cm^{-3})	f_{VCN} (%)	Number of FIDs (seq av)	Time range (μs)	T_2 (ns) HCN	T_2 (ns) HNC	σ (Å^2) HCN	σ (Å^2) HNC
70.3	6.07	0.12	13 (4)	30-150	83.0 (6.3)	55.9 (2.9)	30.4 (3.9)	45.1 (5.1)
29.0	2.82	0.086	13 (4)	10-130	230.6 (5.8)	120.5 (9.8)	36.6 (3.9)	70.0 (9.3)
18.3	3.60	0.11	24 (2)	10-125	239.3 (2.7)	126.2 (4.0)	34.9 (3.7)	66.1 (7.4)
16.6	4.85	0.066	25 (2)	5-125	176.4 (1.8)	78.1 (4.5)	36.8 (4.0)	83.2 (10.1)
9.4	7.43	0.029	20 (2)	25-120	135.1 (1.1)	61.2 (3.5)	41.8 (4.7)	92.2 (11.6)

Table 1 | Experimental conditions and results. The temperature and total density are derived from Pitot measurements and are subject to an estimated maximum uncertainty of 10%. The fractional number density of vinyl cyanide (VCN) is given in percent. The numbers of fitted FIDs and sequential averages taken along the uniform flow contributing to the final values are indicated, as well as the corresponding time range after the laser was fired. Uncertainties in the measured data are given in parentheses. For T_2 these are 95% confidence interval statistical errors from the fits, while for the cross sections these are combined with estimated systematic errors in the temperature and number density.

2 Potential energy surfaces and scattering calculations

A - Potential energy surfaces

The computation of pressure broadening cross sections and rate coefficients takes place within the Born-Oppenheimer approximation for the separation of electronic and nuclear motions.

The ground electronic states of the weakly bound HCN–He and HNC–He systems are singlet states with *A'* reflection symmetry. Within their ground electronic state, HCN and HNC molecules have linear geometries and were therefore considered as a linear rigid rotor. In a recent study, Denis-Alpazar et al.[8] have shown that accounting for the bending motion of HCN during the collision with He barely affects the pure rotational excitation of the molecule compared to the rigid-rotor case. Hence, and because we mostly focus on low temperature collisions (T < 100 K), we anticipate the rigid rotor approach to be highly accurate.

The HCN–He and HNC–He rigid rotor potential energy surfaces (PESs) are described by the two Jacobi coordinates R, the distance from the center of mass of the molecules to the He atom, and θ, the angle between $\vec{R}$ and the molecules bond axis, with θ = 0° corresponding to colinear He–NC/CN–H.

The intermolecular bond distances of the HCN and HNC were frozen at their experimental equilibrium values (r_{HC} = 2.0135 bohr and r_{CN} = 2.1792 bohr for HCN–He; r_{HN} = 1.8813 bohr and r_{NC} = 2.2103 bohr for HNC–He).

The HCN–He and HNC–He PESs were calculated in the supermolecular approach by means of the explicit correlated coupled cluster method including single, double, and perturbative triple excitations [CCSD(T)-F12a][9] with an augmented correlation-consistent polarized valence triple-ζ [aug-cc-pVTZ] basis set[10] (hereafter CCSD(T)-F12/aug-cc-pVTZ). We note that the CCSD(T)-F12/aug-cc-pVTZ method is not size consistent due to the inclusion of noniterative triple excitation. The interaction potential calculated with this method has then been uniformly shifted by subtracting the potential energy at the distance of R = 200 Bohr. The use of the CCSD(T)-F12/aug-cc-pVTZ method is expected to reach the accuracy of PESs deduced from standard coupled cluster approach together with complete basis set (CBS) extrapolation despite the use of a relatively limited atomic basis set.[11]

At all geometries, the Boys and Bernardi counterpoise procedure[12] is used to correct for the basis set superposition error (BSSE). In this procedure the interaction energy is defined by

$$V(R,\theta) = E_{HCN/HNC\ He}(R,\theta) - E_{HCN/HNC}(R,\theta) - E_{He}(R,\theta) \qquad \text{Eq. 1}$$

where the energies of the HCN/HNC and He subsystems are determined with the full (four atoms plus bond functions) basis set.

The values of the radial scattering coordinate R ranged from 3.5 Bohr to 25 Bohr. The angular grid was uniform with a 10° spacing from 0 to 180°.

In order to be used in scattering calculations, the calculated interaction energies were then fitted by means of the procedure described by Werner et al.[13] for the CN–He system. Over the entire grid, the mean relative difference between the analytic fit and the ab initio calculations is less than 0.5%. The final PESs that were used in this study are shown in Supplementary Fig. 1, along with the difference between these two PESs, demonstrating that these two seemingly similar systems indeed have quite different interactions.

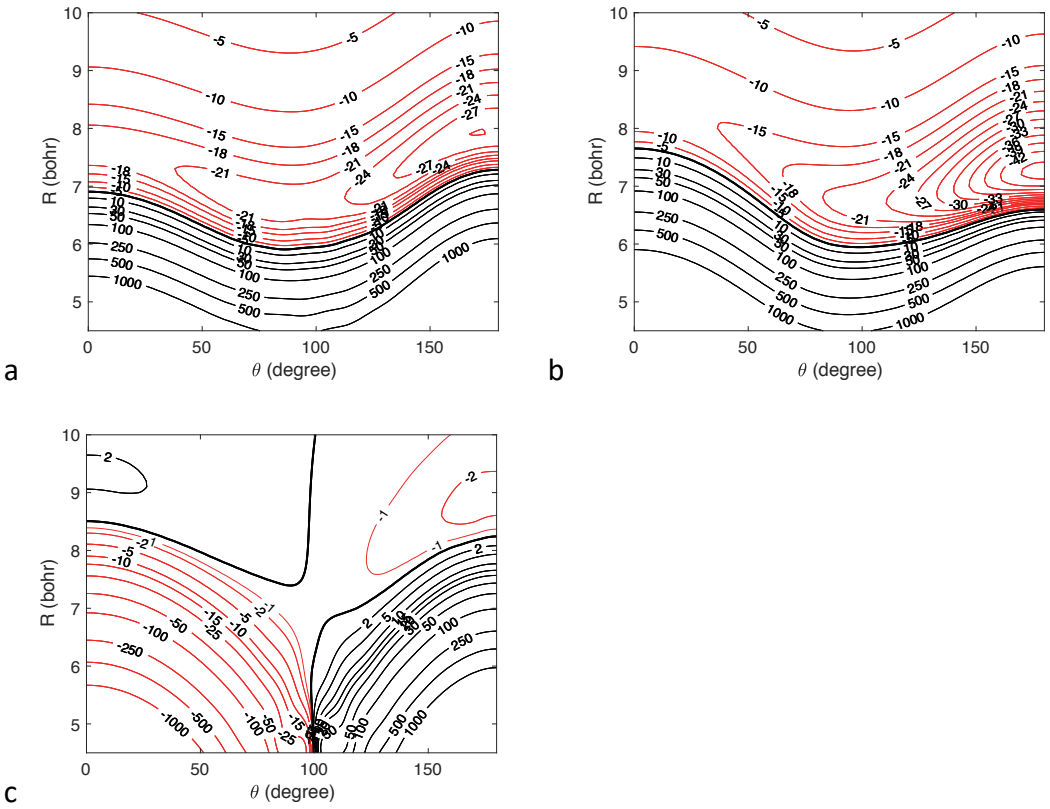

Fig. 1 | Contour plots of calculated PESs (in cm^{-1}). **a**, The HCN–He PES. **b**, The HNC–He PES. **c**, The difference of **a** – **b**.

B – Scattering calculations

In order to perform the dynamical calculations with the MOLSCAT code[14] the PESs were developed over 13 Legendre polynomials:

$$V(R,\theta) = \sum_{L} V_L(R) P_L(\cos\theta). \qquad \text{Eq. 2}$$

A grid of radial terms was built from 2.5 to 30 bohr with a step size of 0.1 bohr. Standard cubic spline interpolations were performed during the course of a MOLSCAT run as well as extrapolations of the form $\frac{C_{L,\alpha}}{R^{\alpha}}$ at long range.

To solve the coupled differential equations, we used the hybrid modified log-derivative Airy propagator[15] as implemented in the MOLSCAT code, the switching point being set at 30 bohr.

Rotational energy levels were obtained with rotational constants B_{HCN} = 1.4772 cm^{-1}, B_{HNC} = 1.512113 cm^{-1} and centrifugal distortion constants D_{HCN} = 2.91 × 10^{-6} cm^{-1}, D_{HNC} = 3.3 × 10^{-6} cm^{-1}.[16] At least five asymptotically closed levels were included in the basis set.

Calculations were conducted for a grid of about 230 relative center of mass kinetic energies E_{kin} ranging from 0.1 to 2000 cm^{-1}.

Having S-matrices in the total angular momentum representation, $\vec{J} = \vec{j} + \vec{\ell}$ ($\vec{\ell}$ refers to the end-over-end angular momentum of the colliding pair) the generalized spectroscopic pressure broadening cross-sections are given in the impact approximation[17,18] by:

$$\sigma^{(1)}\left(j_i, j_f; E_{kin}\right) = \left(\frac{\pi}{k^2}\right) \sum_{J_i J_f \ell \ell'} \left[J_i\right] \left[J_f\right] (-1)^{\ell - \ell'} \begin{Bmatrix} j_i & 1 & j_f \\ J_f & \ell & J_i \end{Bmatrix} \begin{Bmatrix} j_i & 1 & j_f \\ J_f & \ell' & J_i \end{Bmatrix} \quad \text{Eq. S3}$$
$$\times \left[\delta_{\ell\ell'} - < j_i \ell' \left| S^{J_i}(E_{\text{kin}} + E_i) \right| j_i \ell > < j_f \ell' \left| S^{J_f}(E_{\text{kin}} + E_f) \right| j_f \ell >^* \right]$$

where {:::} is a 6*j* symbol, [*J*] stands for 2*J* + 1. 1 is associated with the electric dipole transition from j_i = 0 to j_f = 1, and E_i, E_f are the associated rotational energies (we have omitted all vibrational quantum numbers equal to 0 here). The real part of such cross sections provides the half width at half maximum (HWHM) of a Lorentzian line shape while the imaginary part leads to the line shift.

It can be shown[17] that the real part of this cross section may be split in two contributions:

$$\text{Re}\left(\sigma^{(1)}(j_i, j_f; E_{\text{kin}})\right) = \sigma_{\text{inelastic}} + \text{Re}\left(\sigma^{(1)}_{\text{dephasing}}(j_i, j_f; E_{\text{kin}})\right) \quad \text{Eq. S4}$$

with

$$\sigma_{\text{inelastic}}\left(j_i, j_f; E_{kin}\right) = \frac{1}{2}\left(\sum_{j_i' \neq j_i} \sigma(j_i \rightarrow j_i'; E_{kin}) + \sum_{j_f' \neq j_f} \sigma(j_f \rightarrow j_f'; E_{kin}) \right). \quad \text{Eq. S5}$$

In Eq. S4 the dephasing contribution is due to the elastic events while the inelastic contribution (Eq. S5) is the half sum of standard cross sections out of the levels involved in the transition. The so-called random phase approximation[19] neglects the dephasing contribution resulting from elastic collisions and thus directly relates the pressure broadening coefficients to the inelastic rate coefficients. This would be applicable when the energy level spacing is quite small and the kinetic energy is large compared to the well depth of the PES. Moreover, this approximation is known to work best for large rotational quantum numbers.[20–23] As the present study deals with the j_i = 0 to j_f = 1 transitions of HCN and HNC in helium at low temperatures, the random phase approximation is therefore not applicable. Pressure broadening cross sections for large rotational quantum numbers are mostly sensitive to the repulsive part of the interaction potential and thus show less elastic contribution than those for small rotational quantum numbers which sample the long and short range interactions.

Finally, since measurements are performed at a given temperature, it is necessary to average the pressure broadening cross sections over the Maxwell – Boltzmann distribution in kinetic energies:

$$\sigma^{(1)}(j_i, j_f; T) = \left(\frac{1}{k_B T} \right)^2 \int_0^\infty dE_{kin} E_{kin} \exp(-E_{kin} / k_B T) \sigma^{(1)}(j_i, j_f; E_{kin}) \quad \text{Eq. S6}$$

The current computed cross sections agree quite well with previous calculations[4,24] of pressure broadening cross sections for HCN–He, even if based on different PESs.[25–28]

Supplementary **Fig. 2** displays state-to-state rate coefficients for inelastic rotational energy transfer in collisions of He with HCN and HNC at 10 K, as calculated by Sarrasin et al.,[29] with the application as necessary of the principle of detailed balance.

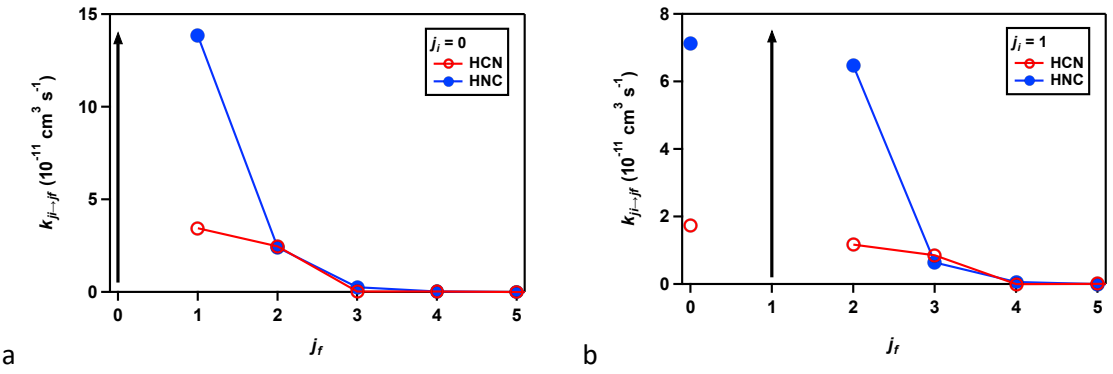

Fig. 2 | Calculated state-to-state rate coefficients for inelastic rotational energy transfer in collisions of He with HCN (open red circles) and HNC (filled blue circles) at 10 K. **a**, Rate coefficients $k_{ji\rightarrow jf}$ from initial state $j_i = 0$. **b**, Rate coefficients $k_{ji\rightarrow jf}$ from initial state $j_i = 1$.

Supplementary references

1. Hays, B. M. *et al.* Design and performance of an E-band chirped pulse spectrometer for kinetics applications: OCS – He pressure broadening. *J. Quant. Spectrosc. Radiat. Transf.* **250**, 107001 (2020).
2. Ahrens, V. *et al.* Sub-Doppler Saturation Spectroscopy of HCN up to 1 THz and Detection of J = 3 —> 2 (4—> 3) Emission from TMC1. *Z. Für Naturforschung A* **57**, 669–681 (2002).
3. DeLucia, F. & Gordy, W. Molecular-Beam Maser for the Shorter-Millimeter-Wave Region: Spectral Constants of HCN and DCN. *Phys. Rev.* **187**, 58–65 (1969).
4. Green, S. Effect of nuclear hyperfine structure on microwave spectral pressure broadening. *J. Chem. Phys.* **88**, 7331–7336 (1988).
5. Carty, D., Goddard, A., Sims, I. R. & Smith, I. W. M. Rotational energy transfer in collisions between CO ($X^1\Sigma^+$, v=2, J=0, 1, 4, and 6) and He at temperatures from 294 to 15 K. *J. Chem. Phys.* **121**, 4671–4683 (2004).
6. Mertens, L. A. *et al.* Rotational energy transfer in collisions between CO and Ar at temperatures from 293 to 30K. *Chem. Phys. Lett.* **683**, 521–528 (2017).
7. Sánchez-González, R., Bowersox, R. D. W. & North, S. W. Simultaneous velocity and temperature measurements in gaseous flowfields using the vibrationally excited nitric oxide monitoring technique: a comprehensive study. *Appl. Opt.* **51**, 1216 (2012).
8. Denis-Alpizar, O., Kalugina, Y., Stoecklin, T., Vera, M. H. & Lique, F. A new ab initio potential energy surface for the collisional excitation of HCN by para- and ortho-H_2. *J. Chem. Phys.* **139**, 224301 (2013).
9. Knizia, G., Adler, T. B. & Werner, H.-J. Simplified CCSD(T)-F12 methods: Theory and benchmarks. *J. Chem. Phys.* **130**, 054104 (2009).
10. Kendall, R. A., Dunning, T. H. & Harrison, R. J. Electron affinities of the first-row atoms revisited. Systematic basis sets and wave functions. *J. Chem. Phys.* **96**, 6796–6806 (1992).
11. Lique, F., Kłos, J. & Hochlaf, M. Benchmarks for the generation of interaction potentials for scattering calculations: applications to rotationally inelastic collisions of C_4 ($X^3\Sigma_g^-$) with He. *Phys. Chem. Chem. Phys.* **12**, 15672 (2010).

12. Boys, S. & Bernardi, F. Calculation of Small Molecular Interactions by Differences of Separate Total Energies - Some Procedures with Reduced Errors. *Mol. Phys.* **19**, 553-(1970).
13. Werner, H., Follmeg, B., Alexander, M. & Lemoine, D. Quantum Scattering Studies of Electronically Inelastic-Collisions of CN ($X^2\Sigma^+$, $A^2\Pi$) with He. *J. Chem. Phys.* **91**, 5425–5439 (1989).
14. Hutson, J. & Green, S. MOLSCAT computer code, version 14, distributed by Collaborative Computational Project No. 6 of the Engineering and Physical Sciences Research Council. *Swindon UK* (1994).
15. Alexander, M. & Manolopoulos, D. A Stable Linear Reference Potential Algorithm for Solution of the Quantum Close-Coupled Equations in Molecular-Scattering Theory. *J. Chem. Phys.* **86**, 2044–2050 (1987).
16. Endres, C. P., Schlemmer, S., Schilke, P., Stutzki, J. & Mueller, H. S. P. The Cologne Database for Molecular Spectroscopy, CDMS, in the Virtual Atomic and Molecular Data Centre, VAMDC. *J. Mol. Spectrosc.* **327**, 95–104 (2016).
17. Ben-Reuven, A. Impact Broadening of Microwave Spectra. *Phys. Rev.* **145**, 7–22 (1966).
18. Shafer, R. & Gordon, R. G. Quantum scattering theory of rotational relaxation and spectral line shapes in H_2–He gas mixtures. *J. Chem. Phys.* **58**, 5422–5443 (1973).
19. DePristo, A. E. & Rabitz, H. The effect of elastic and reorientation collisions on vibration-rotation lineshapes: A semi-empirical approach. *J. Quant. Spectrosc. Radiat. Transf.* **22**, 65–79 (1979).
20. DePristo, A. E. & Rabitz, H. On the use of various scaling theories in the deconvolution of rotational relaxation data: Application to pressure-broadened linewidth measurements. *J. Chem. Phys.* **69**, 902–911 (1978).
21. Thibault, F., Calil, B., Boissoles, J. & Launay, J. M. Experimental and theoretical CO_2–He pressure broadening cross sections. *Phys. Chem. Chem. Phys.* **2**, 5404–5410 (2000).
22. Thibault, F. *et al.* Experimental and theoretical CO_2–Ar pressure-broadening cross sections and their temperature dependence. *Phys. Chem. Chem. Phys.* **3**, 3924–3933 (2001).
23. Faure, A., Wiesenfeld, L., Drouin, B. J. & Tennyson, J. Pressure broadening of water and carbon monoxide transitions by molecular hydrogen at high temperatures. *J. Quant. Spectrosc. Radiat. Transf.* **116**, 79–86 (2013).
24. Ronningen, T. J. & De Lucia, F. C. Helium induced pressure broadening and shifting of HCN hyperfine transitions between 1.3 and 20 K. *J. Chem. Phys.* **122**, 184319 (2005).
25. Green, S. & Thaddeus, P. Rotational Excitation of HCN by Collisions. *Astrophys. J.* **191**, 653 (1974).
26. Atkins, K. M. & Hutson, J. M. The potential energy surface of He–HCN determined by fitting to high-resolution spectroscopic data. *J. Chem. Phys.* **105**, 440–450 (1996).
27. Toczyłowski, R. R., Doloresco, F. & Cybulski, S. M. Theoretical study of the He–HCN, Ne–HCN, Ar–HCN, and Kr–HCN complexes. *J. Chem. Phys.* **114**, 851 (2001).
28. Harada, K., Tanaka, K., Tanaka, T., Nanbu, S. & Aoyagi, M. Millimeter-wave spectroscopy of the internal-rotation band of the He–HCN complex and the intermolecular potential energy surface. *J. Chem. Phys.* **117**, 7041–7050 (2002).

29. Sarrasin, E. *et al.* The rotational excitation of HCN and HNC by He: new insights on the HCN/HNC abundance ratio in molecular clouds. *Mon. Not. R. Astron. Soc.* **404**, 518–526 (2010).